Chinese Journal of Chemical Engineering 82 (2025) 246–255

Contents lists available at ScienceDirect

Chinese Journal of Chemical Engineering

journal homepage: www.elsevier.com/locate/CJChE

Full Length Article

Evaluation of live Cryo-ECT system for liquid nitrogen–vapor nitrogen flow

Zenan Tian [1], Zhiyu Zhang [2, 3], Xiang Li [2], Xinxin Gao [1], Ziru Ren [1], Xiaobin Zhang [1, *]

[1] *Institute of Refrigeration and Cryogenics, Zhejiang University, Hangzhou 310027, China*
[2] *Zhejiang Baima Lake Laboratory Co., LTD, Hangzhou 310027, China*
[3] *Zhejiang Zheneng Aerospace Hydrogen Technology Co., LTD, Hangzhou 310027, China*

A R T I C L E I N F O

Article history:
Received 24 December 2024
Received in revised form
21 February 2025
Accepted 24 February 2025
Available online 8 March 2025

Keywords:
Electrical capacitance tomography
Cryogenic
Flow visualization
Two-phase flow
Artificial neural network

A B S T R A C T

A cryogenic visible calibration and image evaluation facility (VCCIEF) was constructed to assess the effectiveness of electrical capacitance tomography systems in cryogenic conditions, known as Cryo-ECT. This facility was utilized to conduct dynamic, real-time imaging trials with liquid nitrogen (LN2). The actual flow patterns were captured using a camera and contrasted with the imaging outcomes. The capacitance data collected from these experiments were subsequently processed using three distinct methods: linear back projection, Landweber iteration, a fully connected deep neural network, and a convolutional neural network. This allowed for a comparative analysis of the performance of these algorithms in practical scenarios. The findings from the LN2 experiments demonstrated that the Cryo-ECT system, when integrated with the VCCIEF, was capable of successfully executing calibration, generating flow patterns, and performing imaging tasks. The system provided observable, clear, and precise phase distributions of the liquid nitrogen–vaporous nitrogenflow within the pipeline.

1. Introduction

With the increasing attention on the utilization of space resources, the rise of commercial aerospace, and the continuous advancement of space exploration, reusable spacecraft and high-thrust rockets have been continuously developed. The liquid hydrogen (LH2) and liquid oxygen (LO2) propellants have become the mainstream choice for space fuels due to their advantages of high specific impulse, wide thrust range, cleanliness, and no pollution [1]. During the launch, on-orbit operation, and landing process of reusable rockets, monitoring the phase distribution of cryogenic propellants can help obtain their distribution status in the storage tank, ensuring that the pressure, temperature, and propellant content in the tank can maintain the normal function of the rocket engine [2]. However, due to the microgravity environment in the working environment of rocket engines, liquid propellants are prone to floating unsteadily in gas–liquid two-phase states, and traditional pressure or level sensors based on pressure or level measurement are ineffective. Therefore, it is necessary to develop an effective method for inferring the phase distribution of cryogenic fluids to achieve more accurate, reliable, and real-time monitoring of the status of cryogenic liquids.

Electrical capacitance tomography (ECT) technology, as a non-intrusive and non-contact capacitance-based phase distribution measurement technology, has been widely used in real-time phase distribution detection in room-temperature application scenarios [3], such as fluidized-bed [4–6], oil–water transmission pipelines [7], oil and gas pipelines [8,9], and multiphase flow detection [10,11], relying on its advantages of high accuracy, high robustness, low cost, and real-time performance. However, its application in the field of cryogenic fluid is less, and there are few research results to obtain the phase distribution image of cryogenic fluid. The reason is that the low temperature of cryogenic fluid, rapid freezing, and damage to conventional materials inevitably make the cryogenic electrical capacitance tomography (Cryo-ECT) sensor without adaptive design wrinkle and fracture. The difficulties of material selection, fabrication, and processing in ECT systems and the intense boiling of cryogenic fluids at room temperature also pose challenges to calibration, imaging, and evaluation processes. These difficulties require redesigning a high-precision capacitance

* Corresponding author. Institute of Refrigeration and Cryogenics, Zhejiang University, Zheda Road 38th, Hangzhou 310027, China.
E-mail address: zhangxbin@zju.edu.cn (X. Zhang).

https://doi.org/10.1016/j.cjche.2025.02.010
1004-9541/

data acquisition system, a high generalization ability algorithm, and a cryogenic measurement and observation platform for the Cryo-ECT system. As for the imaging algorithm, with the development of ECT technology and improved computer calculation capacity, machine learning (ML) methods have been widely used in ECT inversion problems. The applicability of different network models such as fully connected neural networks [12], convolutional neural networks (CNN) [13,14], long short-term memory (LSTM) networks [15], generative adversarial networks (GAN) [16–18], and other models to ECT problems have been studied. Machine learning algorithms can also be fused to traditional algorithms to optimize while taking physical information into account [19]. It is already practical to select and train deep neural networks as real-time inversion algorithms for ECT systems.

Much preliminary work has been carried out on the Cryo-ECT in recent years. Xie *et al.* [20–22] used the room temperature ECT system and alternative working medium to conduct numerical simulation and room temperature substitution experiment, verifying cryogenic ECT technology's feasibility. Hunt *et al.* [23] pioneered cryogenic experiments by using an ECT system to measure the average dielectric constant of liquid nitrogen and performing content insertion experiments, which is the originator of cryogenic ECT evaluation. Besides, their research of ECT was examined by LH2 [24], and the first image of LH2 was obtained, which is a critical event in the direction of future applications of ECT applications with aerospace storage tanks and so on. Even more recently, their system has made a great achievement in the commercialization of ECT by evaluating a spherical cryogenic ECT imaging system that is already ready for practical use [25]. The sensor performed real-time liquid nitrogen (LN2) imaging experiments and used imaging algorithms to obtain stereoscopic three-dimensional (3D) images of LN2. This is a big step in the cryogenic ECT. After that, Gao *et al.* [26] and Tian *et al.* [27] both used the immersion method to realize the LN2 calibration and measurement in the ECT imaging process, used the preliminary test method and the pre-trained deep neural network to image the measured capacitance value, and obtained a clear and accurate image of liquid nitrogen–vaporous nitrogen (LN2–VN2) two-phase flow.

Despite the extensive research conducted on Cryo-ECT, there is a paucity of literature addressing the evaluation methodologies for Cryo-ECT systems. The assessment of imaging outcomes necessitates a reference to the actual phase distribution, which is inherently challenging to ascertain for cryogenic fluids. At present, it is infeasible to capture the phase distribution through an opaque, closed container, a limitation that Cryo-ECT technology is specifically designed to overcome. A potential resolution involves the fabrication of containers from transparent materials, thereby facilitating the documentation of true flow patterns.

One approach entails the direct immersion method, wherein a cylindrical medium is positioned within the cross-sectional area of the measurement conduit to establish a predefined flow pattern, which can then be photographed. Alternatively, the gravimetric method can be employed to quantify the fluid contained within the vessel. Nevertheless, the unique characteristics of cryogenic fluids pose significant challenges. Upon exposure to ambient temperatures, these fluids are prone to boiling, which complicates the process of recording the intended flow patterns.

In this paper, a visible cryogenic calibration and image evaluation facility (VCCIEF) with a vacuum chamber is designed, fabricated, and used for phase distribution reconstruction experiments of a Cryo-ECT system. The experimental platform can simultaneously meet the installation of a Cryo-ECT sensor and the observation and recording of cryogenic fluid phase distribution, which is used to evaluate the accuracy of imaging results of a Cryo-ECT system. The capacitance data acquisition system (CAU) developed for cryogenic applications collects and transmits capacitance values. A sustained LN2 level drop was recorded. The pre-trained convolutional neural network imaging model is loaded into the imaging program of the host computer for real-time imaging, and the data is recorded. After the experiment, the images are calculated by the other three inversion algorithms and compared with the convolutional neural network model. The results show that the VCCIEF can intuitively complete the experiment and evaluation of the Cryo-ECT system.

2. Cryogenic ECT System

The Cryo-ECT system in this paper is composed of a VCCIEF, sensors, a CAU, the host computer, and additional equipment (Fig. 1). The working mediums designed for the system are LH2, LN2, LO2 (liquid oxygen), and LNG (liquid natural gas). Due to safety considerations, the experimental working medium in this paper is LN2.

The research on electrical capacitance tomography systems in normal temperature and high-temperature application scenarios has been relatively mature, and conventional sensors have been able to meet most of the practical requirements. The special characteristics of cryogenic application scenarios present additional unique challenges for Cryo-ECT systems:

(1) It is difficult to build the test scene. The heat transfer between the cryogenic fluid and the normal-temperature environment will lead to violent boiling so that the preset flow pattern cannot be obtained. At present, the most practical method is to soak the outside of the pipeline in the same working medium, and reduce or even eliminate the heat exchange between the internal working medium and the outside, so as to complete the full field calibration, flow pattern setting, and other work. This is clearly an unprofessional and premature implementation.

(2) The extremely low temperature of the working medium will damage the sensor pipe, electrodes, and other parts, and even break if the material with the uneven thermal expansion is used. For the detection platform needed for scientific research to evaluate the imaging quality, the experimental platform should also be equipped with an observable observation window and a transparent segment after meeting the required conditions of electrical capacitance tomography. It is also difficult to choose the appropriate structure and material for the design and manufacture of the experimental platform.

(3) Failure of the sensor after uncontrollable shrinkage of the material at cryogenic conditions. Due to the difference in the expansion coefficient, the copper pole piece attached to the pipe will contract at low temperatures, resulting in folds and

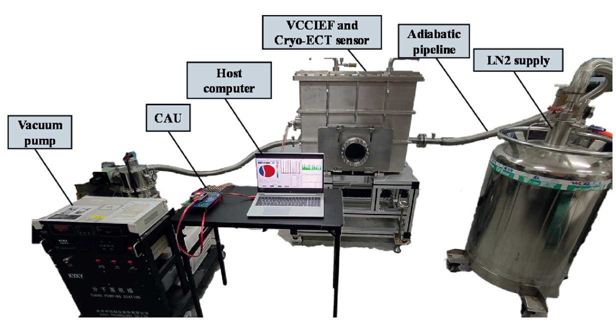

Fig. 1. Cryo-ECT system.

cavities (Fig. 2), which will cause distortion of the capacitor constructed by the sensor and invalidate the calculation model.

(4) The relative permittivity of cryogenic fluid is much smaller than that of normal-temperature fluid. The measurement object of the ECT system is the capacitance value of the working medium between the two electrodes, and the relative dielectric constant ratio of LN2–VN2 is 1.43, while the relative dielectric constant ratio of water–air is 78. This puts forward higher requirements for the measurement accuracy of CAU.

These problems are addressed accordingly by the following methods:

(1) A VCCIEF is designed, manufactured, and debugged (Fig. 3). It greatly reduces the heat exchange between the working medium in the tube and the outside through the vacuum chamber, and can easily complete the empty/full field calibration and the dynamic and static flow pattern preset through the adjustment of the valve and pipeline.

(2) The main body of VCCIEF is made of 304 stainless steel. The transparent pipe in the test section is made of acrylic, which is the result of the selection of glass and other organic materials after trial manufacturing, balancing the processability and the structural strength at cryogenic conditions. The manufacturing process of the observation section needs to eliminate stress to avoid fragmentation after a temperature change. The electrodes and shields of the sensor are realized by a flexible printed circuit (FPC) scheme, which effectively avoids the pole plate wrinkling when increasing the strength.

(3) For cryogenic scenarios, the design of sensors needs to balance the strength of the sensor with high-precision measurement results. From an engineering perspective, using thick metal plates instead of metal electrodes can enhance the strength of the electrodes, effectively ensuring the integrity of the electrodes in various application scenarios. However, thicker metal electrodes can produce more severe fringe effects, which can reduce the precision and sensitivity of the sensor. Therefore, in applications where precision is critical, thinner metal electrodes are often used. The conventional method of using copper foil patches, where large-area metal electrodes have adhered to pipes, can lead to problems due to the difference in thermal expansion coefficients between the two materials. At cryogenic conditions, the metal electrodes can easily wrinkle, form bubbles, or even detach from the pipes. Distortion of the electrodes can cause the sensor to fail completely. Alternative electrode fixation methods must be employed to ensure the structural integrity of the sensor under cryogenic applications. After evaluating and testing the thick metal plate, copper foil patch, cryogenic glue bonding, and other schemes. Fortunately, the FPC can better meet the needs of Cryo-ECT. The thickness of the polyimide film on both sides of the board is 25 μm, which basically does not affect the imaging results, and it is strongly bonded with the copper layer in the manufacturing process, which prevents the copper layer from wrinkle. The copper layer thickness is on the order of micrometers, which also meets the requirements of Cryo-ECT thin plates. Thus, the inherent strength of the FPC is sufficient to overcome the challenges posed by cryogenic conditions. In addition, the attachment of the FPC to the pipeline does not depend on adhesive bonding. For each sensor dimension, a corresponding mounting fixture is employed, utilizing a crimping method for secure fastening. This approach ensures optimal adherence of the sensor to the pipeline during the processes of pre-cooling and rewarming.

(4) Since the traditional patch scheme cannot even maintain the integrity of its main structure under cryogenic conditions, we conducted experiments using a room-temperature substitute working fluid to compare the sampling stability performance between the FPC scheme and the traditional

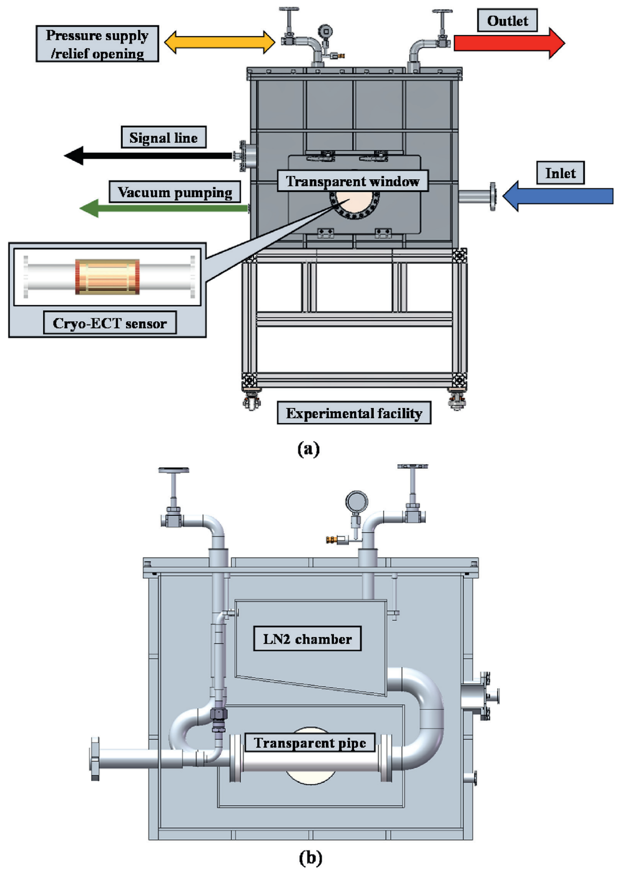

Fig. 3. Visible cryogenic calibration and image evaluation facility (VCCIEF): (a) overall view and (b) sectional view.

Fig. 2. Wrinkles of the patch electrodes after recovery from cryogenic condition.

scheme. Apart from the electrode scheme, all other conditions such as pipeline dimensions and materials, CAU, and imaging software were kept identical for both schemes. For the experiment, a polypropylene particle–air fluid pair was selected as the substitute working fluid. The relative permittivity of polypropylene particles is 1.62, which is close to that of LN2 (1.43) and LNG (1.63). The pipeline has a diameter of DN70, is made of quartz glass, and has a thickness of 2 mm. The CAU uses a ZJU-ECT capacitance acquisition card, developed by Institute of Refrigeration and Cryogenics of Zhejiang University, and all connecting wires are 1-m-long RG178 coaxial cables with SMA connectors. The capacitance sampling results for the two schemes are shown in Fig. 4. The capacitance of a pair of directly opposing electrodes (electrode 1 and electrode 5) in the 8-electrode sensor was measured continuously over time to present the measurement stability of the two sensor configurations. The results indicate that simply by adopting the FPC scheme for the electrodes, the system's capacitance measurement stability can be enhanced by 5 dB.

(5) This is the primary problem encountered in Cryo-ECT research. High-precision CAU suitable for cryogenic fluids has been developed and put into use in the previous preliminary research based on normal temperature replacement working medium.

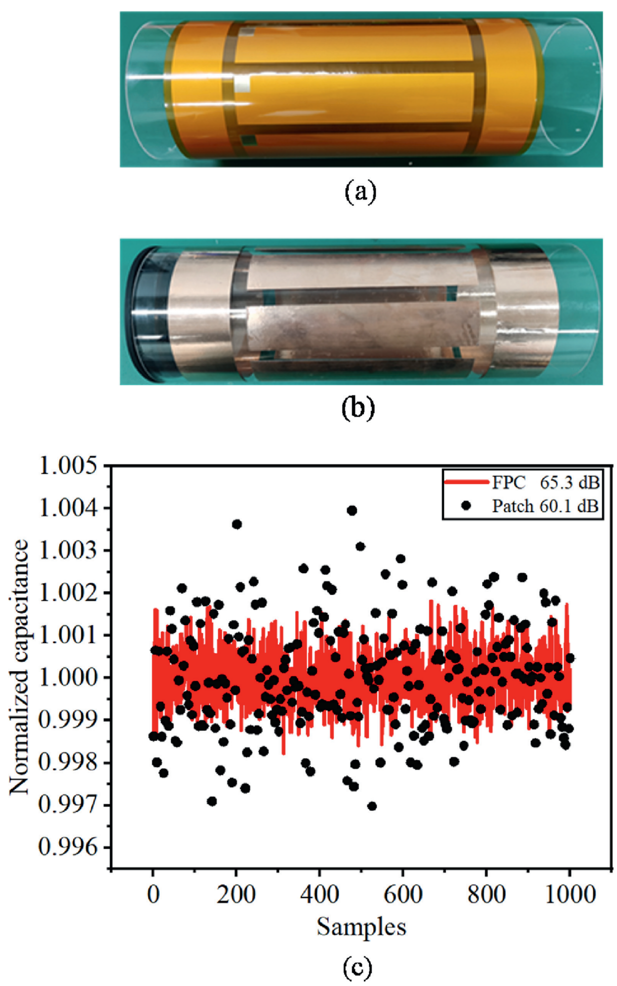

Fig. 4. ECT sensor solution: (a) FPC, (b) patch, and (c) capacitance sampling result.

Based on these designs, the VCCIEF system in this paper can normally complete ECT imaging under cryogenic conditions, and observe the real flow pattern of the working fluid in the pipeline through the observation window, so as to evaluate the imaging quality of the Cryo-ECT system.

The VCCIEF comprises control valves, an LN2 liquid inlet, a vacuum chamber, the test pipeline, and observation windows. The air pressure of the internal pipeline of the experimental platform is controlled by the valve, which acts as the inlet of the VN2 outlet of the internal LN2 vaporization and the external gas supply end. The LN2 liquid inlet is thermally insulated to avoid heat leakage at the inlet, and the external LN2 supply end is connected to the experimental platform through vacuum-insulated pipes and vacuum joints. The vacuum chamber is connected to the external vacuum pump to ensure the insulation of the internal pipeline to avoid the boiling of cryogenic fluid to complete the sensor's full field calibration and measurement process. The test pipe is a transparent pipe to facilitate recording the phase distribution of the fluid inside the test pipe through the observation window to evaluate the inversion imaging results with the Cryo-ECT system, and the inner diameter of the test pipe is 60 mm.

The sensor comprises flexible electrodes integrated with sensing electrodes, a shielding ring, and a shielding cover. CAU is connected to the sensor through a shield line. The CAU in this paper is a subsystem for capacitive data acquisition and preliminary processing. Its workflow is described as follows: The control and processing unit receives signals from the host computer to initiate the sampling process. The measurement signal generation module then produces the excitation signals required for the measurement. The switching module connects the excitation end and the measurement section to the measuring electrodes on the sensor. The signal measurement module performs the capacitance-to-voltage conversion. The sampling module collects the voltage signals, which are then processed by the control and processing unit. This unit performs digital filtering and demodulation to convert the voltage signals into capacitance values. Finally, the communication module sends the processed capacitance values to the host computer *via* wireless or wired communication. The sampling resolution of the CAU is 14 bits, with a capacitance measurement range of 2 pF, and the final imaging frequency is 5 Hz.

Before the experiment, the sensor was fixed on the periphery of the test pipeline. Then, the CAU was connected to the sensor to complete the initial installation of the experimental system. Purge the air inside the pipe with pure N_2 to prevent condensation of water vapor. Then, the vacuum pump is sealed and connected to the exhaust port of the experimental platform. The air pressure in the vacuum chamber is reduced to 10^{-4} Pa at room temperature before LN2 can be introduced. Since a large amount of LN2–VN2 two-phase flow will be generated in the nonadiabatic pipe, and LN2 is required in the full-field calibration process, the additional gas phase generated will take a lot of time. The LN2 flow rate of the standard volume tank delivered by the factory is low and unstable, so it is inappropriate as the LN2 supply end of the experimental platform. Therefore, the LN2 is transferred to a particular storage tank in this experiment. The outlet of the storage tank is adiabatic designed as the experimental platform, and an adiabatic pipe connects the middle to reduce the gas phase content of the LN2 inlet end of the test pipeline. The tank can increase the outlet flow through external pressurization to speed up the experiment process.

At the beginning of the experiment, a pre-cool procedure was conducted. After slowly introducing LN2 into the test pipe, the LN2 inside the test pipe will produce intense boiling. During this process, the parts in contact with the cryogenic fluid, including the test pipe and the sensor, will have small deformation. Due to the adaptive design, the sensor pole plate will not be folded and have a cavity as in the conventional scheme, but the change in capacitance value is inevitable. Therefore, ECT's empty and full field calibration can only be completed after pre-cooling. In addition, the slight deformation of the internal pipe connection during the pre-cooling process will slightly destroy the vacuum degree, and the vacuum chamber pressure will rise to 10^{-3} Pa. The adiabatic characteristics of the vacuum chamber under this pressure can still be maintained, and the fluid in the test pipe basically does not produce boiling after the pre-cooling is completed.

During the experiment, the liquid level inside the test pipeline can be changed by adjusting the tilt angle of the experimental platform, pressure valve, and external air source to realize rapid liquid intake and discharge.

For a cryogenic pipeline system, calibrating the test section is relatively straightforward for empty-field calibration; simply introducing saturated nitrogen vapor after complete pre-cooling is sufficient. However, full-field calibration presents a challenge. The direct immersion method, which involves completely submerging the test section horizontally or vertically into the liquid phase, does not align with actual operating conditions, as cryogenic fluids typically only exist within containers. Moreover, without proper thermal insulation, heat leakage from the container surface can interfere with the full-field calibration process due to the formation of surrounding bubbles. This necessitates the use of a vacuum chamber. Thus, the VCCIEF's vacuum chamber approach simulates the working environment of the Cryo-ECT sensor and also allows for convenient empty and full-field calibrations through valve operations.

The vacuum chamber addresses the issue of creating full-field calibration conditions, but the visualization feature of the VCCIEF enhances the verification process. During observations without thermal insulation, water vapor condensation near the cryogenic fluid can significantly interfere with the acquisition of the true liquid surface. Even with methods to isolate water vapor, it is difficult to clearly obtain the true phase distribution. The VCCIEF uses transparent materials to construct the test pipeline and has observation viewports on the vacuum chamber, allowing for multi-angle observation of the cryogenic fluid inside the pipeline. This unobstructed recording of the true flow pattern can be compared with the imaged results to assess the imaging performance of the Cryo-ECT system.

In addition to this, the VCCIEF also set up an LN2 chamber above the experimental pipeline, allowing liquid nitrogen to flow into the pipeline from top to bottom, which can be seen in Fig. 3(b). This design facilitates the implementation of full-field calibration more conveniently.

3. Reconstruction Method

The Cryo-ECT system applied an 8-electrode sensor scheme, and the sampled data in each frame consists of 28 mutual capacitors generated by the combination of these electrodes in pairs. Each frame of the phase distribution image is divided into 1836 2D triangular cells using the finite element method (FEM). The sampling data of each frame and the phase distribution image are mapped to each other. Generating sampled data from phase distribution images is known as a forward problem, and vice versa is an inverse problem. The forward problem is a well-posed problem that Maxwell's equations can solve, and the accuracy of the solution depends on the fineness of the meshing, which is considered to be a solved problem. The inverse problem is underdetermined, and the solution is not unique, depending on the solution method. The solution algorithms range from the original linear algorithms, such as linear back projection (LBP) and iterative algorithms, to the popular machine learning models in recent years. This paper uses two classical linear algorithms, LBP and Landweber iterative, with two pre-trained deep learning models, a fully connected deep neural network (FCDNN), and a convolutional neural network (CNN). Since the main creative work of this paper is real-time Cryo-ECT system imaging, in order to avoid too long a computation time, this paper does not use a too complex deep network model.

3.1. Linear algorithm

(1) LBP algorithm

A discretized formulation of the forward problem to calculate the mutual capacitance can be simplified as

$$\boldsymbol{C} = \boldsymbol{S}\boldsymbol{E} \tag{1}$$

$\boldsymbol{C}$ is an $M \times 1$ normalized capacitance value vector, and M is the number of capacitances in a data frame, which is 28 in this work. $\boldsymbol{E}$ is an $N \times 1$ normalized dielectric permittivity distribution vector, which is to be calculated in the inverse problem. N is the number of FEM cells in the computational domain, which is 1836 in this work. $\boldsymbol{S}$ is an $M \times N$ normalized sensitivity.

The LBP algorithm can be established as follows.

$$\boldsymbol{E} = \boldsymbol{S}^{\mathrm{T}}\boldsymbol{C}\left[\mathrm{diag}\left(\boldsymbol{S}^{\mathrm{T}}\boldsymbol{I}\right)\right]^{-1} \tag{2}$$

where $\boldsymbol{I} = (1\ 1 \cdots 1)^{\mathrm{T}}$. The critical idea of this algorithm is that the sensitivity field is not a matrix, and $\boldsymbol{C}$ cannot be directly obtained by multiplying both sides of the equation by $\boldsymbol{S}^{-1}$. Instead, in this algorithm, $\boldsymbol{S}^{-1}$ is replaced with $\boldsymbol{S}^{\mathrm{T}}$.

The LBP algorithm is the fastest and most universal method for the ECT inversion algorithm with limited accuracy. It can be used as a preliminary validation of the system and as an initial value for other algorithms.

(2) Landweber iteration

The Landweber iterative algorithm is developed based on the steepest descent method. Its iterative expression can be described as

$$\boldsymbol{E}_{k+1} = \boldsymbol{E}_k + \alpha_k \boldsymbol{S}^{\mathrm{T}}(\boldsymbol{C} - \boldsymbol{S}\boldsymbol{E}_k) \tag{3}$$

Taking α_k as the independent variable, the minimum value of $\|\boldsymbol{E}_{k+1}\|_2^2$ appears when the partial derivative is 0 and the optimal iteration step size [28] is

$$\alpha_k = \frac{\left\|\boldsymbol{E}_k^{\mathrm{T}}\widehat{\boldsymbol{S}}\right\|_2^2}{\left\|\widehat{\boldsymbol{S}}\widehat{\boldsymbol{S}}^{\mathrm{T}}\boldsymbol{E}_k\right\|_2^2} \tag{4}$$

3.2. Machine learning method

The machine learning (ML) model can directly map the nonlinearity between the measured capacitance vector $\boldsymbol{C}$ and the dielectric permittivity distribution vector $\boldsymbol{E}$.

$$\boldsymbol{E} = \mathrm{ML}(\boldsymbol{C}) \tag{5}$$

In this paper, the imaging of ECT is regarded as a supervised regression problem, and each deep learning network model is trained by the forward problem calculation. For imaging scenarios involving just a single flow pattern, using this kind of flow pattern to train the network can undoubtedly obtain the best improvement of reconstruction results in theory. However, the actual imaging scenario is not the preset single-flow type. Due to the noise of the measurement system, non-standard flow patterns, and other factors, the characteristics of capacitance data measured by real imaging may be very different from those trained by the deep learning model. So the model needs to have good generalization ability. Apart from the structure of the model, the configuration of training samples is also an important way. The sample set of the deep learning model involved in this paper uses 60000 sets of capacitance–permittivity sample pairs, involving flow patterns including stratified, 1 bar, 2 bar, 3 bar, column, loop flow, and their anti-phase flow patterns.

(1) Fully connected deep neural network

The fully connected deep neural network (FCDNN) is a basic neural network structure known as a Densely Connected Neural Network. In an FCDNN, each layer of neurons is fully connected to all neurons in the previous layer, which means that each neuron receives the output of all neurons in the last layer as input and produces its output signal to pass to the next layer. The basic principle of the fully connected neural network is to train through the backpropagation (BP) algorithm. By constantly adjusting the weights and biases of the neurons, the error between the network output and the actual value is minimized.

The FCDNN in this paper is a 6-layer network consisting of an input, output, and four hidden layers (Fig. 5). The input layer receives capacitance data of 28×1. This usually represents a grayscale image, which has a width of 28. This is followed by four fully connected layers, each of which is followed by a ReLU function for adding nonlinearity. The number of nodes in these layers is 50, 200, 500, and 2000, respectively. After the last fully connected layer, a dropout layer is added with a dropout probability of 0.5. This means that each node in that layer has a 50% chance of being randomly "switched off" during training, which helps prevent overfitting. Finally, the output layer has 1836 nodes. Before the output layer, a sigmoid activation function is added.

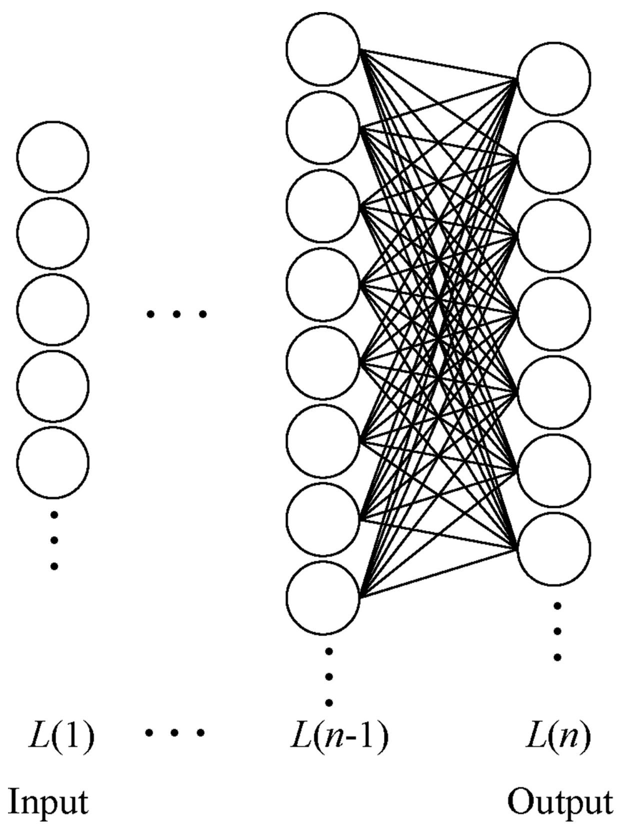

Fig. 5. Scheme of FCDNN.

(2) Convolutional neural network

The convolutional neural network (CNN) extracts features of input images through convolution operation and has shown good feature learning ability in the field of ECT imaging. The basic structure of the CNN includes an input layer, convolutional layer, pooling layer, fully connected layer, and output layer, which is shown in Fig. 6. Among them, the convolutional layer is the core of the convolutional neural network, which extracts the features of the input data through convolution operation. Pooling layers are used to reduce the dimensionality of the data, reducing computation and the risk of overfitting. The fully connected layer is used to integrate the features extracted by the convolutional layer and the pooling layer to output the final imaging result. Through the transformation of different convolution kernels, the network combines the low-level features into a high-level feature representation and can learn and extract the internal laws and patterns of the input capacitance data.

Convolutional neural networks also need to use backpropagation and optimization algorithms to continuously adjust the weights and biases of neurons during the training process to minimize the error between the output and the actual value.

For the convolutional neural network trained in this paper, first, the 28×1 capacitance data vector needs to be converted into 3D data, that is, the size of the input layer is defined to be $28 \times 1 \times 1$. After that, there are multiple modules. The first layer of each convolutional module is a convolutional layer, which is followed by a ReLU activation layer. The filter size of the convolutional layer is 3×1, and the number of filters per convolutional layer is increasing (from 5 to 500). Zeros are added to the edges of the input data through the padding mechanism so that the size of the output feature map is the same as the input. Following each activation layer is a pooling layer with a pooling window size of 2×1 and a step size of one. Since the step size is 1, this means that the pooling operation does not actually reduce the height of the feature map, but only a bit in the width, which may also remain the same due to the Padding mechanism. After multiple convolutional and pooling layers, the network contains three fully connected layers with 2000, 5000, and 1836 nodes. After that, a sigmoid activation layer is used. Because the sigmoid function limits the output between 0 and 1, it conforms to the grayscale range of the ECT output image.

This paper uses the Adam method as the optimizer for both network models.

4. Numerical Experiment

In order to evaluate the performance of each algorithm and determine whether it can be used in the actual LN2–VN2 real-time imaging scene, a numerical simulation experiment was carried out after the models were trained. The experiment simulates the imaging results of each preset flow pattern. Since it is a numerical experiment, the imaging results can be compared with the preset flow pattern to obtain three quantitative parameters: correlation coefficient (CC), image error (IE), and void fraction error (VFE) [27]. The closer the CC is to 1, the smaller the IE and VFE are, and the closer the imaging results are to the preset flow pattern. The

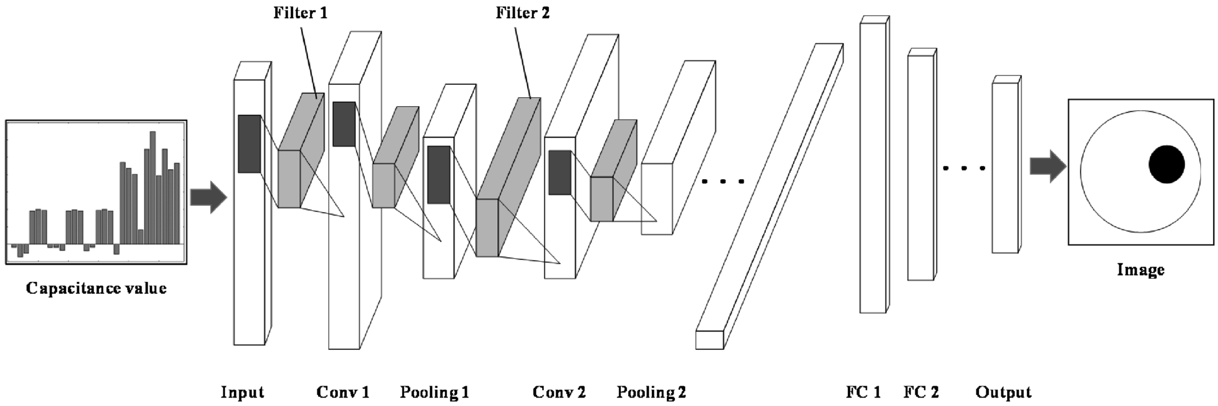

Fig. 6. Scheme of CNN.

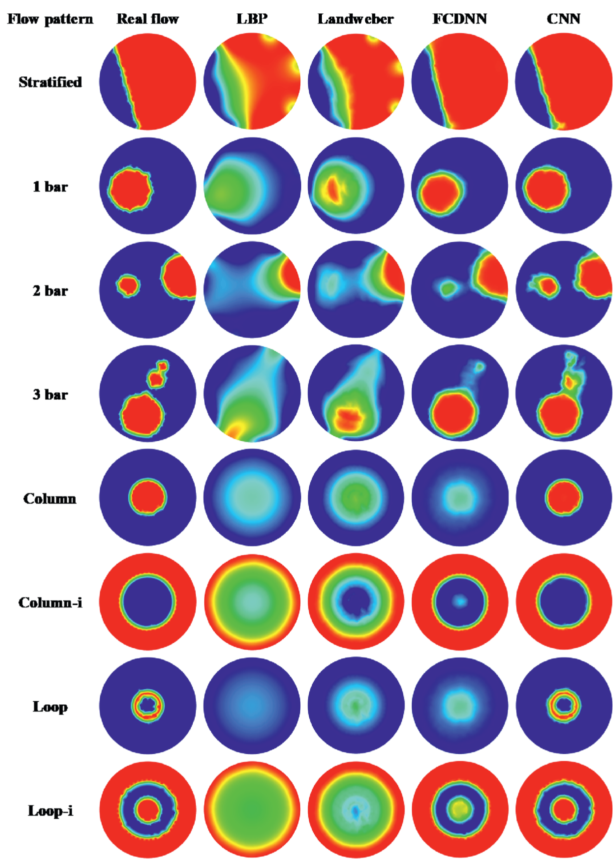

Fig. 7. Reconstructed images for different algorithms in numerical experiment.

imaging results are shown in Fig. 7, where red represents LN2 and blue represents VN2, while the presentation of these quantitative comparison data is shown in Figs. 8–10. These parameters are classified according to different flow patterns in the test set and averaged to show the imaging differences of the algorithm on different flow patterns. Through them, the imaging effect of the algorithm can be measured from multiple dimensions.

From these results, it can be observed that the imaging performance of the four algorithms improves with the complexity of the algorithm in most cases at all levels, but the simple FCDNN may be the worst in terms of the imaging metrics for a specific flow pattern. This may be because the structure of FCDNN is too simple in deep neural networks to perform sample fitting well. On the contrary, CNN has confirmed its superiority in image imaging at all levels and can cover various flow patterns with superior imaging performance such as 3 bar and loop. It is used as the actual LN2–VN2 imaging algorithm.

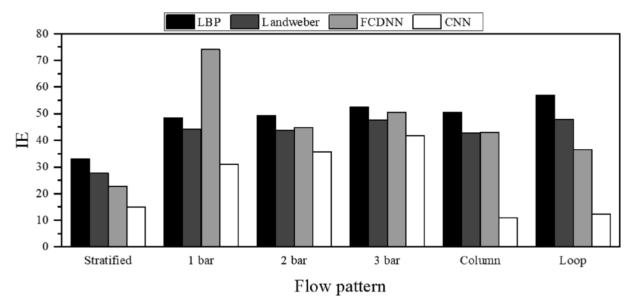

Fig. 9. IE of algorithms in each flow pattern.

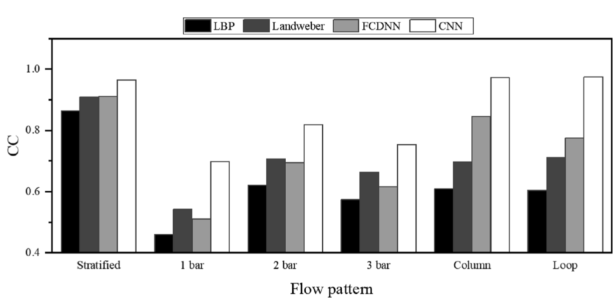

Fig. 8. CC of algorithms in each flow pattern.

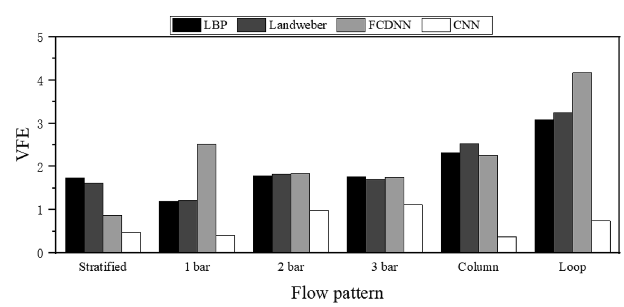

Fig. 10. VFE of algorithms in each flow pattern.

5. Experiment Results

A dynamic cryogenic experiment was conducted in this work on the proposed Cryo-ECT system.

Firstly, N_2 is used for purging at room temperature, and then a small amount of LN2 is introduced into the internal pipeline of the test bed for pre-cooling. At this time, the surface of LN2 will boil vigorously, and continuous rising bubbles are generated on the side of the transparent pipeline. When LN2 in the tube is no longer boiling, it indicates that the pre-cooling step has been completed. At this time, the inside of the experimental pipeline is filled with saturated VN2, and the empty field calibration step is carried out.

After the inside of the test pipeline is fully filled with LN2, which is the full field calibration procedure, after pressure adjustment, the recording begins. The LN2 liquid level surges, relying on the external N2 source at room temperature to provide pressure, and the LN2 inside the experimental pipeline is quickly drained until the pipeline is pure VN2. The algorithm used for real-time inversion by the imaging software is a pre-trained CNN model with an imaging frequency of 5 Hz. The recorded time series data is saved as a*.txt* file, and the change in the cavitation rate is calculated according to the inversion results of the CNN model. The cavitation rate-time change diagram is drawn, as shown in Fig. 11.

The time series data recorded by void fraction (VF) change during a drainage event is saved as a*.txt* file. The change of VF is calculated according to the inversion results of the CNN model, and the VF—time change diagram is drawn, as shown in Fig. 11. The stable VF = 0 segment at the beginning is the full field stage, and the final close to 100% is the empty field. The intermediate VF rising stage is the VN2 discharge stage. Because the draining process through the external pressure is not stable, the VF curve's slope is inconsistent.

In addition to this, the LBP, Landweber, and FCDNN methods were used for secondary imaging after the experiment. At the same time, according to the timestamp, look up the camera recorded at that time and compare it with the imaging results.

The real flow pattern, the CNN real-time imaging results, and the secondary imaging results are shown in Fig. 12. In previous publications, the real image is mapped to the cells of the computational domain and then compared with the inversion image under the flow pattern quantitatively and qualitatively. The accuracy of the inversion image is indicated by image analysis parameters such as correlation coefficient and image error.

Since this experiment is a dynamic test, the real flow pattern is not a stationary stratified flow like the static test, with fluctuations and surge, which cannot be directly mapped into the computational domain as in the previous operation. Therefore, only real dynamic images and imaging results of each algorithm at a few moments are shown in this paper.

Although there is no precise comparison of quantitative parameters, the difference in performance of the individual algorithms on the Cryo-ECT system is intuitive. Among these imaging methods, the CNN model is undoubtedly the most accurate. The performance of the traditional linear algorithm is based on physical information, and it is reliable in most conditions. Even if the most precise imaging results cannot be obtained, it still performs well in the preliminary judgment. The drawback is the unavoidable artifacts at the periphery of the computational domain, which can be in the gas or liquid phases. The other is the relatively fuzzy phase interface boundary.

The reliability of the machine learning method depends on the generalization ability under the model parameter setting and the quality of the training sample. It will produce good results in the range of model fitting, such as P1, P2, and P5 in the FCDNN results. Its error will be uncontrollable and produce relatively chaotic results, such as P3 in FCDNN results, or identify as other popular, such as P7 in FCDNN, combining laminar flow patterns and artifacts to identify as 1 bar flow.

Therefore, the application of machine learning methods in Cryo-ECT should use a model with strong enough generalization. Obviously, FCDNN generally has poorer generalization ability than CNN, as verified by experimental results. The reason is that each neuron in FCDNN is connected to all neurons in the previous layer, leading to a large number of parameters and a tendency to overfit, especially when training data is limited. Although various mechanisms are employed to avoid this, the results of the cryogenic experiments show otherwise. In contrast, CNN significantly reduces the number of parameters through the design of convolutional and pooling layers. The convolutional kernels in the convolutional layers share weights across different positions of the input data, which not only reduces the number of parameters but also enables the model to better capture the relationships between input capacitance data. Additionally, the pooling layers reduce the size of feature maps through down-sampling, lowering model complexity and extracting invariant features.

The imaging results of CNN are also not perfect, and a relatively choppy phase interface can be seen. The reasons are as follows: Firstly, the mesh size is not small enough, so this problem will not be noticed when the phase interface is blurred, but the transition band of the CNN imaging result is small, and the shortcomings of

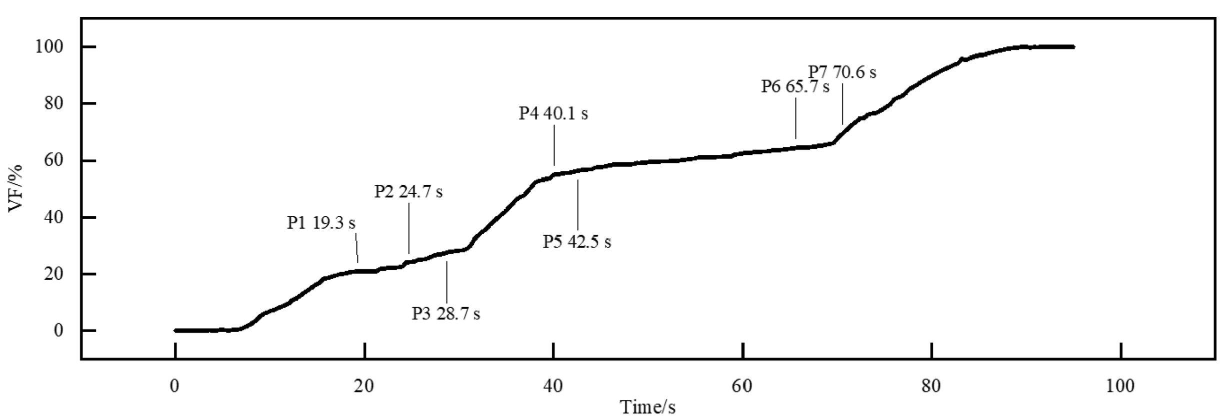

Fig. 11. Calculated VF change during a water drainage event.

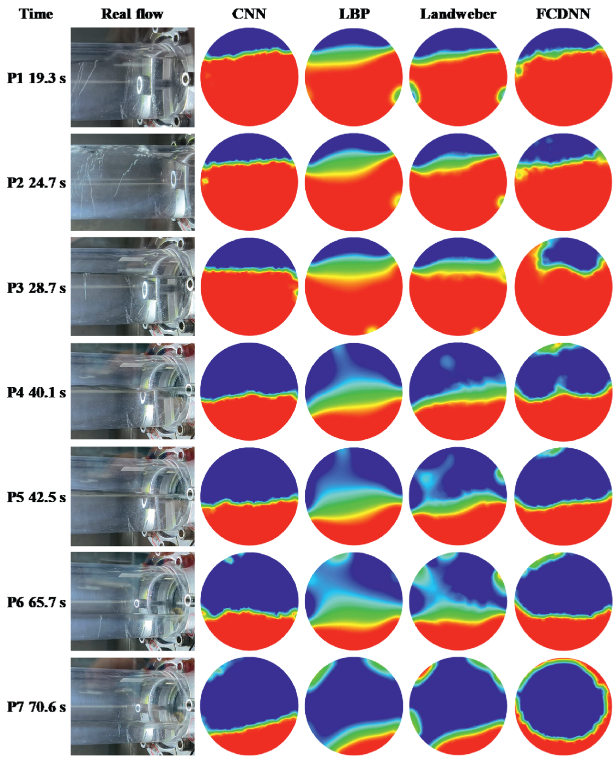

Fig. 12. Photos and reconstructed images for different algorithms.

the triangular mesh interface cannot be fully fitted under the laminar flow pattern will be more obvious. Secondly, there is noise in the capacitance data obtained from the actual sampling.

6. Conclusions

The VCCIEF designed and fabricated in this work is a successful platform. This scheme can serve as a mounting platform for a Cryo-ECT system, used for testing and evaluation of the Cryo-ECT system during the research and development phase. The platform overcomes the problem of difficult observation of the liquid surface of cryogenic fluids that existed in previous studies using direct immersion methods or other methods. The design of the vacuum chamber effectively avoids the frosting of the observation interface or the obstruction by opaque materials. This allows for precise and timely synchronous recording of the real liquid surface and imaging results during the imaging process, which can be used to assess the performance of the Cryo-ECT system installed on the platform. The construction of the pipeline system also effectively reduces the contact opportunities between the testing process and the cryogenic working fluid, thereby significantly enhancing safety. In summary, VCCIEF can complete the procedures of empty field calibration, full field calibration, dynamic flow pattern setting, and flow pattern recording in the imaging process of LN2–VN2 two-phase flow ECT.

The Cryo-ECT system assessed in this paper also effectively addresses the structural failure of traditional ECT sensors at cryogenic conditions, solving the availability of Cryo-ECT from a hardware perspective. Moreover, the adaptive design of the CAU improves the measurement accuracy.

The Cryo-ECT system, together with VCCIEF, completed this experiment's real-time dynamic imaging of cryogenic fluid phase distribution and recorded an LN2 draining process starting from the full field. The calculated VF value can correspond to the process, and the inversion image can also correspond to the real phase distribution. The performance of the traditional linear algorithm and two machine learning models on cryogenic fluid imaging is also compared, which shows the superiority of the CNN model in the actual imaging of Cryo-ECT. The imaging results also show that machine learning methods are mature and accurate enough for the Cryo-ECT system. Meanwhile, the traditional linear algorithm can not be abandoned, and the imaging results of different algorithms can be displayed simultaneously as multiple observations in the actual imaging, ensuring that a single algorithm is misleading to the measurement results. Among them, the result of the traditional linear algorithm is an important basis for judgment.

The Cryo-ECT imaging process also reflects the need for improvement of the experimental platform. The LN2 inlet of the experimental platform requires special vacuum insulation joints and pipes and LN2 transfer, which takes up more preparation time. Additional equipment can be reduced by using built-in LN2 storage tanks and controlling the flow of internal pipes through valves. The integration of CAU is not enough, and imaging still needs a computer platform. The use of embedded processing units and imaging systems will reduce the scale of electronic equipment and facilitate the promotion and use in the engineering stage. These are the next improvement work.

These findings underscore the importance of having a robust experimental platform during the instrument's development phase, the efficacy of employing a vacuum jacket for Cryo-ECT performance assessments, and the demonstrated superiority of CNN in actual Cryo-ECT imaging scenarios. Our results also highlight that CNN outperforms traditional linear algorithms in imaging quality, making it a reliable addition to imaging software for enhanced Cryo-ECT system performance.

The following conclusion can be drawn.

(1) To meet the full-field calibration conditions, the Cryo-ECT facility must be designed with vacuum insulation.
(2) FPC electrodes perform better than traditional patch solutions at low temperatures and can meet cryogenic conditions.
(3) Compared with traditional algorithms based on sensitivity fields and FCDNN, CNN has better imaging accuracy.

CRediT Authorship Contribution Statement

Zenan Tian: Writing – review & editing, Writing – original draft, Software, Formal analysis, Data curation, Conceptualization. Zhiyu Zhang: Methodology, Conceptualization. Xiang Li: Methodology, Conceptualization. Xinxin Gao: Visualization, Data curation. Ziru Ren: Visualization, Data curation. Xiaobin Zhang: Validation, Supervision, Resources, Funding acquisition.

Declaration of Competing Interest

The authors declare that they have no known competing financial interests or personal relationships that could have appeared to influence the work reported in this paper.

Acknowledgements

This work was supported by the National Natural Science Foundation of China (51976177) and the National Key Research and Development Program of China (2022YFB4000047).

References

[1] X. Gao, Z. Tian, X. Zhang, Review on the study of theory and method of electrical capacitance tomography of cryogenics propellant, *Phys. Fluids* 35 (5) (2023) 053308.

[2] M.L. Meyer, J.W. Hartwig, S.G. Sutherlin, A.J. Colozza, Recent concept study for cryogenic fluid management to support opposition class crewed missions to Mars, *Cryogenics* 129 (2023) 103622.

[3] A. do Nascimento Wrasse, E.N. dos Santos, M.J. da Silva, H. Wu, C. Tan, Capacitive sensors for multiphase flow measurement: A review, *IEEE Sens. J.* 22 (22) (2022) 21391–21409.

[4] H.G. Wang, W.Q. Yang, Application of electrical capacitance tomography in circulating fluidised beds—A review, *Appl. Therm. Eng.* 176 (2020) 115311.

[5] X.X. Li, A.J. Jaworski, X.A. Mao, Bubble size and bubble rise velocity estimation by means of electrical capacitance tomography within gas–solids fluidized beds, *Measurement* 117 (2018) 226–240.

[6] D.Y. Yang, L.J. Liu, W.X. Feng, Experimental investigation of an internally circulating fluidized bed with 32-electrode electrical capacitance volume tomography, *Measurement* 127 (2018) 227–237.

[7] K. Perera, W.A.S. Kumara, F. Hansen, S. Mylvaganam, R.W. Time, Comparison of gamma densitometry and electrical capacitance measurements applied to hold-up prediction of oil–water flow patterns in horizontal and slightly inclined pipes, *Meas. Sci. Technol.* 29 (6) (2018) 065102.

[8] A. Alzoghaiby, M. Albagami, S.A. Aldosari, Z. Almutairi, F.M. Al-Alweet, M. Shoaib, S.A. Alshebeili, Adaptive filtering techniques for velocity estimation of tomographic electric capacitance signals of two-phase gas/oil flows, *Flow Meas. Instrum.* 77 (2021) 101866.

[9] S.M. Salehi, H. Karimi, R. Moosavi, A.A. Dastranj, Different configurations of capacitance sensor for gas/oil two phase flow measurement: An experimental and numerical study, *Exp. Therm. Fluid Sci.* 82 (2017) 349–358.

[10] Y.L. Lin, Y. Xu, H.G. Wang, Investigation of gas/oil/water distribution based on electrical capacitance and microwave tomography, in: 2021 5th International Conference on Imaging, Signal Processing and Communications (ICISPC), Kumamoto, Japan, IEEE, 2021, pp. 21–29.

[11] Q. Wang, M. Wang, K. Wei, C.H. Qiu, Visualization of gas–oil–water flow in horizontal pipeline using dual-modality electrical tomographic systems, *IEEE Sens. J.* 17 (24) (2017) 8146–8156.

[12] J. Zheng, L.H. Peng, A deep learning compensated back projection for image reconstruction of electrical capacitance tomography, *IEEE Sens. J.* 20 (9) (2020) 4879–4890.

[13] H. Zhu, J.T. Sun, J. Long, W.B. Tian, S.J. Sun, L.J. Xu, Deep image refinement method by hybrid training with images of varied quality in electrical capacitance tomography, *IEEE Sens. J.* 21 (5) (2021) 6342–6355.

[14] J. Zheng, H.C. Ma, L.H. Peng, A CNN-based image reconstruction for electrical capacitance tomography, in: 2019 IEEE International Conference on Imaging Systems and Techniques (IST), IEEE, Abu Dhabi, United Arab Emirates, 2019.

[15] Z.Q. Xu, F. Wu, L.Y. Zhu, Y. Li, LSTM model based on multi-feature extractor to detect flow pattern change characteristics and parameter measurement, *IEEE Sens. J.* 21 (3) (2021) 3713–3721.

[16] H.M. Gao, S.C. Ku, X.H. Jian, Identification of two-phase flow patterns based on capacitance data of electrical capacitance tomography with semi-supervised generative adversarial network, *Rev. Sci. Instrum.* 94 (10) (2023) 104705.

[17] W. Deabes, A.E. Abdel-Hakim, K.E. Bouazza, H. Althobaiti, Adversarial resolution enhancement for electrical capacitance tomography image reconstruction, *Sensors* 22 (9) (2022) 3142.

[18] Z.H. Xia, Z.Q. Cui, Y.X. Chen, Y.F. Hu, H.X. Wang, Generative adversarial networks for dual-modality electrical tomography in multi-phase flow measurement, *Measurement* 173 (2021) 108608.

[19] H. Mousazadeh, N. Tarabi, J. Taghizadeh-Tameh, A fusion algorithm for mass flow rate measurement based on neural network and electrical capacitance tomography, *Measurement* 231 (2024) 114573.

[20] H.J. Xie, T. Xia, Z.N. Tian, X.D. Zheng, X.B. Zhang, A least squares support vector regression coupled linear reconstruction algorithm for ECT, *Flow Meas. Instrum.* 77 (2021) 101874.

[21] H.J. Xie, H. Chen, X. Gao, X.D. Zheng, X.Q. Zhi, X.B. Zhang, Theoretical analysis of fuzzy least squares support vector regression method for void fraction measurement of two-phase flow by multi-electrode capacitance sensor, *Cryogenics* 103 (2019) 102969.

[22] H.J. Xie, L. Yu, R. Zhou, L.M. Qiu, X.B. Zhang, Preliminary evaluation of cryogenic two-phase flow imaging using electrical capacitance tomography, *Cryogenics* 86 (2017) 97–105.

[23] A. Hunt, I. Rusli, M. Schakel, A. Kenbar, High-speed density measurement for LNG and other cryogenic fluids using electrical capacitance tomography, *Cryogenics* 113 (2021) 103207.

[24] P. Behruzi, A. Hunt, R. Foster-Turner, A. Fischer, Testing an Electrical Capacitance Tomography Sensor in Liquid Hydrogen, AIAA SCITECH 2023 Forum, National Harbor, MD & Online. AIAA, 2023.

[25] M.D. Green, R. Foster-Turner, A. Hunt, A.M. Ramirez-Mancebo, S.C. Lieber, J.W. Hartwig, D. Moxey, A. Tafuni, Flight-ready electrical capacitance tomography SMARTTS tank for use with cryogenics, *Exp. Therm. Fluid Sci.* 154 (2024) 111144.

[26] X.X. Gao, Z.N. Tian, L.M. Qiu, X.B. Zhang, A hybrid deep learning model for ECT image reconstruction of cryogenic fluids, *Flow Meas. Instrum.* 87 (2022) 102228.

[27] Z.N. Tian, X.X. Gao, L.M. Qiu, X.B. Zhang, Experimental imaging and algorithm optimization based on deep neural network for electrical capacitance tomography for LN2–VN2 flow, *Cryogenics* 127 (2022) 103568.

[28] S. Liu, L. Fu, W.Q. Yang, Optimization of an iterative image reconstruction algorithm for electrical capacitance tomography, *Meas. Sci. Technol.* 10 (7) (1999) L37–L39.